

ChemComm

Accepted Manuscript



This is an *Accepted Manuscript*, which has been through the Royal Society of Chemistry peer review process and has been accepted for publication.

Accepted Manuscripts are published online shortly after acceptance, before technical editing, formatting and proof reading. Using this free service, authors can make their results available to the community, in citable form, before we publish the edited article. We will replace this *Accepted Manuscript* with the edited and formatted *Advance Article* as soon as it is available.

You can find more information about *Accepted Manuscripts* in the [Information for Authors](#).

Please note that technical editing may introduce minor changes to the text and/or graphics, which may alter content. The journal's standard [Terms & Conditions](#) and the [Ethical guidelines](#) still apply. In no event shall the Royal Society of Chemistry be held responsible for any errors or omissions in this *Accepted Manuscript* or any consequences arising from the use of any information it contains.

Cite this: DOI: 10.1039/c0xx00000x

www.rsc.org/xxxxxx

ARTICLE TYPE

Li₃VO₄ Anchored Graphene Nanosheets for Long-Life and High-Rate Lithium-Ion Batteries†

Zelang Jian,^a Mingbo Zheng,^b Yanliang Liang,^a Xiaoxue Zhang,^a Saman Gheyfani,^a Yucheng Lan,^c Yi Shi^b and Yan Yao^{a,d*}

5 Received (in, XXX) Xth XXXXXXXXXX 20XX, Accepted Xth XXXXXXXXXX 20XX
DOI: 10.1039/b000000x

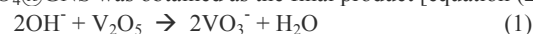
Li₃VO₄ nanoparticles embedded in graphene nanosheets (Li₃VO₄@GNS) were obtained using a sol-gel method. The composite presents excellent high-rate performance with a stable capacity of 133 mAh/g at 50C and long-life performance with capacity retention rate of 63.1% after 5000 cycles at 5C.

Lithium-ion batteries (LIBs) have been widely used as power sources for portable electronics with potential applications in electric vehicles and large-scale energy storage devices because of their high energy density, high power density, and environmentally friendly features.¹ Graphite is commonly used as anode materials in most commercial LIBs. However, graphite reaches almost 0 V vs. Li⁺/Li at the end of the discharge process,² at which potential dendritic lithium could grow on the anode surface and leads to safety issues.³ Spinel Li₄Ti₅O₁₂ has attracted wide attention as a promising anode material because of its minimal volume change and relatively high voltage during Li⁺ insertion/extraction.⁴ Although Li₄Ti₅O₁₂ shows good cyclability and high safety, it suffers from low capacity (175 mAh/g) and relatively high intercalation potential at 1.54 V vs. Li⁺/Li.⁵ Recently, Li₃VO₄ has attracted increasing attention as a new anode material with suitable intercalation potential between 0.5 and 1 V vs. Li⁺/Li. The potential is lower than that of Li₄Ti₅O₁₂ and higher than that of graphite. The theoretical capacity of Li₃VO₄ is 394 mAh/g, corresponding to a two-Li intercalation into the Li₃VO₄ structure. Furthermore, Li₃VO₄ has high ionic conductivity and has been studied as an ionic conductor for many years.^{6,7} In contrast, the electronic conductivity of Li₃VO₄ is quite low and results in large resistance polarization and poor rate performance.⁸ To improve the electrochemical performance, improving the electronic conductivity and reducing particle size by growing inorganic nanoparticles on graphene has been proved to be an effective approach.^{9,10}

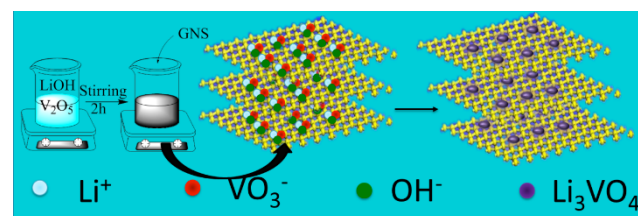
In this study, we synthesized Li₃VO₄@GNS nanocomposite as a novel anode material for LIBs, where Li₃VO₄ nanoparticles were embedded in graphene nanosheets (GNS). This nanocomposite was obtained using a sol-gel method. Li₃VO₄ formed as fine crystals uniformly on GNS. Li₃VO₄@GNS delivers excellent rate performance and cycling stability. Pristine Li₃VO₄ simply mixed with GNS was also prepared for

comparison. Electrochemical impedance spectroscopy (EIS) was used for better understanding of the function of the composite.

50 Graphite oxide (GO) was synthesized from natural graphite powders using a modified Hummers method.¹¹ After thermal exfoliation of GO, GNS with porous structure was obtained, which provide space to accommodate other materials.¹² Furthermore, the large amount of functional groups on the surface of GNS can supply adsorption sites for different ions.¹² Therefore, Li₃VO₄@GNS composite can be prepared using the sol-gel method with the schematic illustration shown in Figure 1. First, V₂O₅ powders were added into LiOH solution in stoichiometric quantity of forming Li₃VO₄. After dissolving V₂O₅, a yellow solution was obtained with the formation of VO₃⁻ ions, after which GNS was added and stirred overnight to obtain black sediment. After calcination at 600 °C for 2 h, Li₃VO₄@GNS was obtained as the final product [equation (2)].



More details of experimental procedure are given in the supplementary information.



70 **Figure 1** Schematic illustration of the synthesis procedure of Li₃VO₄@GNS composite.

Li₃VO₄ crystallizes in a cubic structure with a space group of Pnm2₁, where O ions form hexagonal close-packed structure, while Li and V ions occupy 3/8 and 1/8 of tetrahedral interstitial sites, respectively (Figure S1). X-ray diffraction (XRD) patterns of pristine Li₃VO₄ and Li₃VO₄@GNS samples are shown in Figure 2a. The diffraction peaks of both samples can be indexed into an orthorhombic Li₃VO₄ structure (JCPDS No. 38-1247). The LiO₆ and VO₆ tetrahedron are corner-shared to form a three dimensional structure. Estimation from the XRD peaks using the Scherrer equation revealed particle sizes of 53 nm and 34 nm for pristine Li₃VO₄ and Li₃VO₄/GNS, respectively. For the

$\text{Li}_3\text{VO}_4@\text{GNS}$ sample, a bump exists at around 25° , which could be assigned to that of the GNS. Raman spectroscopy is a powerful tool for characterizing graphitic structures. The peaks between $200 \sim 500 \text{ cm}^{-1}$ and $750 \sim 1000 \text{ cm}^{-1}$ are attributed to the Raman peaks of Li_3VO_4 , which are in good agreement with the findings of previous work.^{8a} However, the intensity of these peaks for $\text{Li}_3\text{VO}_4@\text{GNS}$ decreases sharply, indicating that Li_3VO_4 is well embedded inside the GNS and thus hardly detectable by Raman spectroscopy. Two additional peaks located at 1345 cm^{-1} and 1595 cm^{-1} for $\text{Li}_3\text{VO}_4@\text{GNS}$ sample are attributed to the characteristic Raman peaks of the D-band and G-band of the graphitic material, respectively. The 26 wt.% content of GNS in the $\text{Li}_3\text{VO}_4@\text{GNS}$ composite was estimated from thermogravimetric analysis (Figure S2).

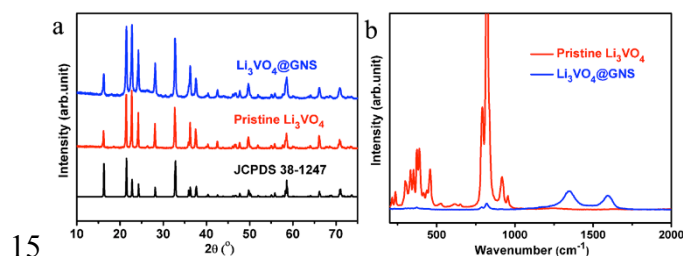


Figure 2 (a) XRD patterns and (b) Raman spectra of the pristine Li_3VO_4 and $\text{Li}_3\text{VO}_4@\text{GNS}$ composite.

Scanning electron microscopy (SEM) and transmission electron microscopy (TEM) were used to further study the morphology of two samples. Figure 3a shows pristine Li_3VO_4 particles with two different sizes: bigger particles around 0.5-1 μm and smaller ones around 20-50 nm. Considering the XRD results in Figure 2a, the sol-gel synthesis of Li_3VO_4 produce nanoparticles around 20-50 nm. During the calcination step, some of these nanoparticles aggregate to form large particles. Figure 3b shows the interplanar spacing of the crystals of 0.37 nm, corresponding to the (101) plane. In the presence of GNS, the aggregation of Li_3VO_4 nanoparticles becomes more restricted with mostly small nanoparticles in 10-30 nm and less percentage of larger particles around 500 nm (Figure S5). $\text{Li}_3\text{VO}_4@\text{GNS}$ sample also shows a high degree of crystallinity. The displayed crystalline interplanar spacing of 0.39 nm in Figure 3d corresponds to the (011) planes. The presence of $\text{Li}_3\text{VO}_4/\text{GNS}$ composite was further confirmed by the selected area electron diffraction (SAED) pattern (inset of Figure 3d) owing to its characteristic diffraction rings and spots. The diffraction rings correspond to (002) and (004) planes of GNS. The diffraction spots are indexed as crystals of Li_3VO_4 , which are in good agreement with the XRD results.

The electrochemical performance of the $\text{Li}_3\text{VO}_4@\text{GNS}$ composite was analysed in CR2032 coin cells. Figure 4a shows the first three cycles of discharge/charge curves at a rate of 0.5C (note that 0.5C refers to two Li insertion into Li_3VO_4 per formula unit in 2 h). The initial discharge/charge capacity is 744/486 mAh/g, resulting in an irreversible capacity loss of 42%, which might be due to the formation of the solid electrolyte interface (SEI) film. The subsequent coulombic efficiency is improved over cycles; the coulombic efficiency for the second cycle can reach 94.6%. Cyclic voltammetry

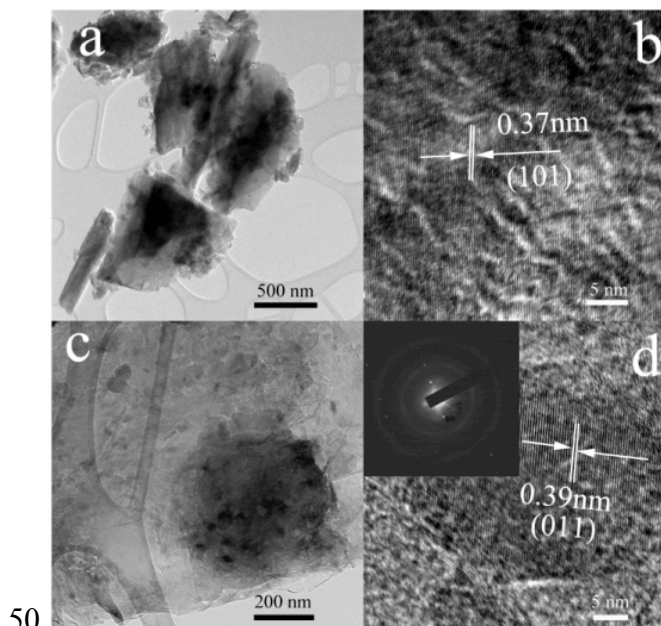


Figure 3 (a) TEM image of pristine Li_3VO_4 ; (b) HRTEM image of pristine Li_3VO_4 ; (c) TEM image of $\text{Li}_3\text{VO}_4@\text{GNS}$ composite; (d) HRTEM image of $\text{Li}_3\text{VO}_4@\text{GNS}$ composite; inset is the corresponding SAED pattern.

measurement was also performed and the corresponding first three cycles of the CV curves at a scan rate of 0.05 mV/s are shown in Figure 4b. For the first cycle curve, two reduction peaks are found at 0.62 and 0.52 V, which shift to 0.86 and 0.53 V in the subsequent cycles, indicating a phase transformation during Li insertion. Only one broad oxidation bump around 1.34 V can be observed in the first three cycles, indicating similar lithium extraction mechanism.

We also investigated the rate performance of the $\text{Li}_3\text{VO}_4@\text{GNS}$ composite. Stable capacity are observed at about 400, 350, 310, 256, 215, 175, and 133 mAh/g at rates of 0.5C, 1C, 2C, 5C, 10C, 20C and 50C, respectively (Figure 4c), with ~90% of which coming from Li_3VO_4 instead of GNS at all rates (Figure S6). Compared with the pristine Li_3VO_4 sample, simply mixed with 26 wt.% of GNS as conductive additive, $\text{Li}_3\text{VO}_4@\text{GNS}$ composite shows higher capacity, especially at high rates. For instance, $\text{Li}_3\text{VO}_4@\text{GNS}$ composite delivers a capacity of about 133 mAh/g at 50C (8 mAh/g contributed from GNS), whereas the capacity of pristine Li_3VO_4 is almost zero. The significantly improved rate performance of this composite structure is attributed to the presence of small Li_3VO_4 particles and close contact between Li_3VO_4 particles and GNS, which reduce Li^+ ion diffusion distance and increase the electronic conductivity. Figure 4d shows the EIS results of pristine Li_3VO_4 and $\text{Li}_3\text{VO}_4@\text{GNS}$ before and after discharge/charge. The Nyquist plots show one semicircle and a quasi-straight line (which represents the Warburg impedance, Z_w), which are associated with the charge transfer resistance (R_{ct}) and impedance of Li^+ diffusion in solid materials, respectively. Moreover, the values of R_{ct} for $\text{Li}_3\text{VO}_4@\text{GNS}$ are obviously lower than those of pristine Li_3VO_4 , indicating better electronic contact of the $\text{Li}_3\text{VO}_4@\text{GNS}$ electrode. The values of R_{ct} decrease after discharging/charging both electrodes, indicating a

decrease in resistance after cycling. The long-life performance of $\text{Li}_3\text{VO}_4@\text{GNS}$ is shown in Figure 4e. The capacity can be maintained at 163 mAh/g at a rate of 5C after 5000 cycles, which is close to the theoretical capacity of $\text{Li}_4\text{Ti}_5\text{O}_{12}$. A capacity retention of about 63.1% and a coulombic efficiency close to 100% has been obtained after activation at 0.5C for five cycles. The excellent long-life performance can be ascribed to the unique structure, in which Li_3VO_4 nanoparticles are well embedded inside GNS to form a structurally stable composite material (Figure 7S).

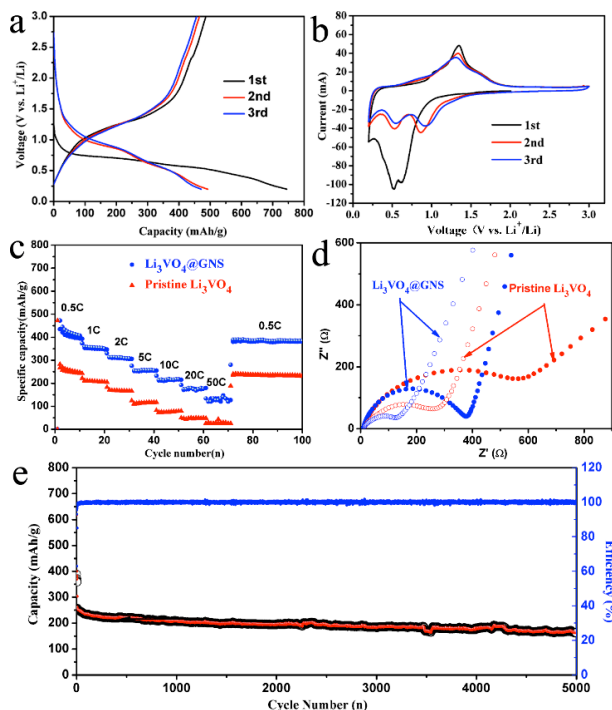


Figure 4 (a) Galvanostatic discharge and charge profiles of the $\text{Li}_3\text{VO}_4@\text{GNS}$ composite in the voltage range of 0.2 ~ 3 V vs Li/Li^+ at a rate of 0.5C; (b) Corresponding cyclic voltammetry of the $\text{Li}_3\text{VO}_4@\text{GNS}$ at a scan rate of 0.05 mV/s; (c) Discharge and charge capacities of the pristine Li_3VO_4 and $\text{Li}_3\text{VO}_4@\text{GNS}$ composite at different C-rates, (d) Nyquist plots for the pristine Li_3VO_4 and $\text{Li}_3\text{VO}_4@\text{GNS}$ composite before (solid) and after (hollow) first cycling; (e) long-life performance of $\text{Li}_3\text{VO}_4@\text{GNS}$ composite at 5C. All capacity calculation is based on the mass of Li_3VO_4 .

In summary, we have designed a facile method to fabricate $\text{Li}_3\text{VO}_4@\text{GNS}$ composite, in which Li_3VO_4 nanoparticles (about 10~30 nm) are well embedded in GNS. This novel $\text{Li}_3\text{VO}_4@\text{GNS}$ composite has been investigated as an anode material for LIBs. The composite presents excellent high-rate performance with a stable capacity of 133 mAh/g even at 50C. After 5000 cycles at a rate of 5C, its capacity maintained at 163 mAh/g, which is 63.1% retention of the original reversible capacity. This result can be attributed to the formation of a conducting network of mixed Li^+ ions and electrons, as well as the protection provided by GNS in terms of reducing the side reaction between Li_3VO_4 and electrolyte. These excellent

properties make $\text{Li}_3\text{VO}_4@\text{GNS}$ composite structure a promising anode candidate for LIBs.

We acknowledge the support from the National Science Foundation (CMMI-1400261) and Robert A. Welch Professorship at TeSUH (E-0001).

40 Notes and references

^a Department of Electrical and Computer Engineering and Materials Science and Engineering Program, University of Houston, Houston, TX 77204, USA. E-mail: yyao4@uh.edu

^b Nanjing National Laboratory of Microstructures, School of Electronic Science and Engineering, Nanjing University, Nanjing 210093, China.

^c Department of Physics and Engineering Physics, Morgan State University, Baltimore, MD 21254, USA

^d Texas Center for Superconductivity, University of Houston, Houston, TX 77204, USA

† Electronic Supplementary Information (ESI) available. See DOI: XXXXXX

1 (a) M. Armand and J.-M. Tarascon, *Nature*, 2008, **451**, 652; (b) C.-X. Zu and H. Li, *Energy & Environmental Science*, 2011, **4**, 2614.

2 (a) T. Nagaura and K. Tozawa, *Prog. Batteries Solar Cells*, 1990, **9**, 209; (b) K. Xu, *Chemical Reviews*, 2004, **104**, 4303.

3 G. Zheng, S. W. Lee, Z. Liang, H.-W. Lee, K. Yan, H. Yao, H. Wang, W. Li, S. Chu and Y. Cui, *Nature Nanotechnology*, 2014, **9**, 618.

4 (a) Z. Jian, L. Zhao, R. Wang, Y.-S. Hu, H. Li, W. Chen and L. Chen, *RSC Adv.*, 2012, **2**, 1751; (b) V. Etacheri, R. Marom, R. Elazari, G. Salitra and D. Aurbach, *Energy & Environmental Science*, 2011, **4**, 3243.

5 L. El Ouatani, R. Dedryvere, C. Siret, P. Biensan and D. Gonbeau, *Journal of the Electrochemical Society*, 2009, **156**, A468.

6 H. Li, X. Liu, T. Zhai, D. Li and H. Zhou, *Advanced Energy Materials*, 2013, **3**, 428.

7 K. Gaur, A. Pathak and H. Lal, *Journal of Materials Science*, 1988, **23**, 4257.

8 (a) Y. Shi, J.-Z. Wang, S.-L. Chou, D. Wexler, H.-J. Li, K. Ozawa, H.-K. Liu and Y.-P. Wu, *Nano letters*, 2013, **13**, 4715; (b) Y. Shi, J. Gao, H. D. Abruña, H. J. Li, H. K. Liu, D. Wexler, J. Z. Wang and Y. Wu, *Chemistry-A European Journal*, 2014, **20**, 5608; (c) Q. Li, J. Sheng, Q. Wei, Q. An, X. Wei, P. Zhang and L. Mai, *Nanoscale*, 2014, in press

9 (a) M. Zheng, D. Qiu, B. Zhao, L. Ma, X. Wang, Z. Lin, L. Pan, Y. Zheng and Y. Shi, *RSC Advances*, 2013, **3**, 699; (b) L.-H. Hu, F.-Y. Wu, C.-T. Lin, A. N. Khlobystov and L.-J. Li, *Nature Communications*, 2013, **4**, 1687.

10 D. Wang, D. Choi, J. Li, Z. Yang, Z. Nie, R. Kou, D. Hu, C. Wang, L. V. Saraf and J. Zhang, *ACS nano*, 2009, **3**, 907.

11 D. C. Marcano, D. V. Kosynkin, J. M. Berlin, A. Sinitskii, Z. Sun, A. Slesarev, L. B. Alemany, W. Lu and J. M. Tour, *ACS nano*, 2010, **4**, 4806.

12 Z. Jian, B. Zhao, P. Liu, F. Li, M. Zheng, M. Chen, Y. Shi and H. Zhou, *Chemical Communications*, 2014, **50**, 1215.